ACS OMEGA

http://pubs.acs.org/journal/acsodf

Article

2D Ag Ion-Loaded Anionic Nanosheets for Polymer-Based Film with Durable Antibacterial Activities

Shi-Yu Yang, Kuan Wu, Ying Zhang, Hao-Xuan Liu, Ping Li, Chao Wu,* and Ke-lu Yan*

Cite This: *ACS Omega* 2022, 7, 33858−33865

Read Online

ACCESS | Metrics & More | Article Recommendations

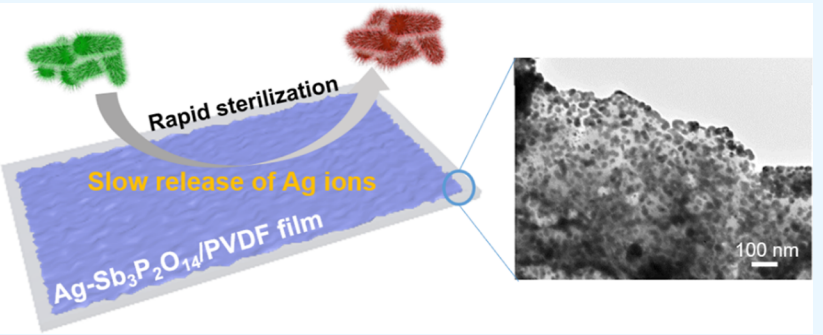

ABSTRACT: Silver (Ag) has been demonstrated to have excellent performance to kill bacteria, fungi, and some viruses because it can release positively charged Ag ions with highly antibacterial and antifungal activities. However, effectively controlling the slow release of Ag ions is the key to preparing high-performance Ag-based antibacterial agents, which remains a challenge. In this work, we have developed a new Ag-based antibacterial agent composed of Ag ions loaded on 2D anionic 2D $Sb_3P_2O_{14}^{3-}$ nanosheets (denoted as Ag-$Sb_3P_2O_{14}$). 2D anionic nanosheets not only adsorb a large amount of Ag ions but also control their slow release through electrostatic interaction between nanosheets and Ag ions. 2D Ag-$Sb_3P_2O_{14}$ nanofillers enable excellent high antibacterial activities for the poly(vinylidene fluoride) (PVDF) film composites against microorganisms including *Escherichia coli* and *Staphylococcus aureus*. Moreover, the PVDF membrane with 5 wt % 2D Ag-$Sb_3P_2O_{14}$ nanofillers can kill almost all bacterial after 50 times washing, demonstrating its excellent durable antibacterial activities. This work opens up a new and promising route to durable Ag-based antibacterial agents for polymer-based composites.

1. INTRODUCTION

Poly(vinylidene fluoride) (PVDF) has gained wide applications as membrane and film materials owing to its unique physicochemical properties such as high thermal stability, high mechanical strength, and excellent membrane formation.[1−3] Such properties make PVDF a good candidate to prepare polymer-based antibacterial membranes and films for applications in packaging materials, textiles, and water treatment.[3,4] However, previous studies demonstrated that pure PVDF membrane is easily adsorbed by various biocontaminants including bacteria. The adsorbed bacteria are able to multiply and clone to form a sticky biofilm on the PVDF membranes and films, which can further adsorb more contaminants.

Recently, much effort has been devoted to develop PVDF-based films with excellent antibacterial property to prevent the accumulation of the surface contaminants. Various organic and inorganic fillers have been reported to incorporate in the PVDF membrane to increase its antibacterial, such as Ag nanoparticles,[5,6] functional graphene,[7−9] MoO_3 nanowires,[10] nano ZnO powder,[11] TiO_2 nanoparticles,[12,13] and metal organic frameworks.[14,15] Comparted to other metal and metal oxides, Ag has demonstrated excellent antibacterial and antifungal activities due to its high cytotoxicity against a wide variety of microorganisms.[16] Although the antibacterial mechanism of Ag is not clear,[17] recent studies have demonstrated that the Ag ions released from the Ag metal are responsible for the antibacterial activities.[18] For example, the released Ag ion interacts with the sulfhydryl groups from the enzymes and proteins of the cell membrane,[19] leading to protein deactivation and bacterial death. The antibacterial effect of the Ag metal is dependent on the concentration of the released Ag ion around the bacteria, which means that ultrasmall Ag nanoparticles have antibacterial property, much better than bulk Ag and micro-sized Ag particles because of

Received: May 2, 2022
Accepted: August 25, 2022
Published: September 14, 2022

https://doi.org/10.1021/acsomega.2c02718
ACS Omega 2022, 7, 33858−33865

their high surface area. However, the Ag nanoparticles are easy to agglomerate when they are separated from aqueous solutions. In order to prevent the aggregation of ultrasmall Ag nanoparticles in the solid state, they are usually anchored on other inorganic nanoparticles, nanowires, and 2D nanosheets with a high surface area,[20−22] which can significantly improve the antibacterial activities.

Apart from achieving Ag ions from the isolated Ag nanoparticles, silver salts can release Ag ions to kill microorganisms. Generally, insoluble silver salt powder releases Ag ions too slowly and soluble silver salt powder releases Ag ions too fast, which renders them not suitable as antibacterial agents. In order to control the slow release of Ag ions, they are fixed at the organic polymer matrix and inorganic nanoparticles by chelation and adsorption.[23−25] For instance, Fe_3O_4 nanoparticles with functional groups were reported to adsorb the Ag ions, which can serve as an antibacterial agent to enhance the antibacterial performance of carrageenan-based packing films.[26] However, the loading of Ag ions on the nanoparticle is not high owing to the low surface area. In principle, the adsorption amount and sustained release of Ag ions are dependent on the surface area of substrates and the interaction between the Ag ion and substrates. Comparted to nanoparticles, 2D ultrathin nanosheets with a large aspect ratio and a high surface area have potential as a candidate to load more Ag ions. Moreover, the electrostatic adsorption has a stronger interaction force than simple physical adsorption, which not only increases the adsorption amount but also reduces the release rate of Ag ions. Therefore, it is reasonable to assume that the negatively charged 2D nanosheets are an excellent adsorption candidate to achieve a high-performance Ag ion-based antibacterial agent.

Herein, we report a novel antibacterial agent composed of Ag ions adsorbed on 2D $Sb_3P_2O_{14}^{3-}$ nanosheets (denoted as Ag-$Sb_3P_2O_{14}$), which can significantly improve the durable antibacterial activities of the PVDF membrane. 2D $Sb_3P_2O_{14}^{3-}$ nanosheets show graphene-like nanostructures with a high surface area and a strong negative charge and can adsorb large amounts of Ag ions and control their slow release. As a result, the PVDF film with 5% Ag-$Sb_3P_2O_{14}$ exhibits excellent antibacterial activities against *Escherichia coli* and *Staphylococcus aureus* and has a good antibacterial effect even after 50 times washing.

2. EXPERIMENTAL SECTION

2.1. Materials. KNO_3 (Adamas, 99%), Sb_2O_3 (Adamas, 99%), $NH_4H_2PO_4$ (Adamas, 99.99%), HNO_3 (diluted, 65−68 wt %), and $AgNO_3$(Adamas, 99.8%) were purchased from Sinopharm Chemical.

2.2. Preparation of 2D $H_3Sb_3P_2O_{14}$ Nanosheets. 2D $H_3Sb_3P_2O_{14}$ nanosheets could be synthesized based on previous literature.[27,28] First, 2.66 g of KNO_3, 5.06 g of Sb_2O_3, and 3.51 g of $NH_4H_2PO_4$ were mixed and heated up to obtain $K_3Sb_3P_2O_{14}$ powder. After that, 4 g of $K_3Sb_3P_2O_{14}$ powder was treated with 500 mL of nitric acid (8 M) for 12 h, which was repeated three times to complete the proton exchange reaction and provide $H_3Sb_3P_2O_{14}$ bulks, followed by exfoliation via vigorous stirring in a pure water solution. Finally, the suspension was centrifuged under 3000 rpm for 30 min, and the non-exfoliated bulk material was removed to obtain ultrathin 2D $H_3Sb_3P_2O_{14}$ nanosheets.

2.3. Preparation of Ag-$Sb_3P_2O_{14}$ Nanosheets. Ag-$Sb_3P_2O_{14}$ nanosheet powder was synthesized by dissolving $AgNO_3$ in a colloidal suspension of $H_3Sb_3P_2O_{14}$ in water (0.26 wt %). Once the dispersed $H_3Sb_3P_2O_{14}$ nanosheets were contacted by the dissolved $AgNO_3$, a flocculation phenomenon occurred immediately because the negatively charged $Sb_3P_2O_{14}^{3-}$ attracts the positive Ag^+ to form Ag-$Sb_3P_2O_{14}$.The Ag-$Sb_3P_2O_{14}$ nanosheet powder was collected by filtration, washed with deionized water, and dried at 80 °C.

2.4. Preparation of Ag-$Sb_3P_2O_{14}$/PVDF Thin Film. The Ag-$Sb_3P_2O_{14}$/PVDF thin film was prepared by casting the slurry of PVDF (M_w = 1000000) mixed with 5, 10, 15, and 20 wt % of Ag-$Sb_3P_2O_{14}$ powder on the glass pane. The pure PVDF film and the PVDF composite film with 10 wt % $H_3Sb_3P_2O_{14}$ were prepared as a contrast group. Finally, these materials were collected after being dried at 80 °C for 8 h.

2.5. Characterization of Ag-$Sb_3P_2O_{14}$/PVDF. The surface morphologies of the samples were conducted by scanning electron microscopy (SEM, JSM-7500F) combined with energy-dispersive X-ray spectroscopy (EDS, JEOL, JSM-7610F), transmission electron microscopy (TEM, JEOL 2100F), and optical imaging (SHOT ON MI 6X). The structural properties and chemical composition analysis for samples were performed using X-ray diffraction (XRD, Rigaku D/Max-2200V PC) and X-ray photoelectron spectroscopy (XPS, Thermo Scientific K-Alpha).

2.6. Antibacterial Activities. *Escherichia coli* (*E. coli*, ATCC25922) and *Staphylococcus aureus* (*S. aureus*, ATCC6538) served as model bacteria for evaluating the antibacterial activities of the Ag-$Sb_3P_2O_{14}$/PVDF film.

Zone of inhibition test was applied to qualitatively measure the antibacterial activities of samples. First, the bacterial suspension was grown in Luria-Bertani (LB) agar medium at 37 °C for 24 h. Then, the suspension was diluted to a density of approximately 5×10^7 CFU/mL by mixing with culture medium, followed by uniformly spreading 100 μL of diluted suspension over the agar plates. As for examining the inhibition zone, the samples were put on the center of agar plates and cultured at 37 °C for 24 h. Finally, a digital camera was utilized to directly record the inhibition zone.

As for the bacterial inhibition rate test, the bacterial suspension was diluted to a density of approximately 1×10^8 CFU/mL, and then the suspension was centrifuged for 3 min × 3 times with PBS solution. 0.075 g of Ag-$Sb_3P_2O_{14}$/PVDF thin film was then introduced into the bacterial suspension (7×10^6 CFU/mL) and incubated at 37 °C. Besides, the culture medium without bacteria served as the blank controlled sample, and the bacteria suspension without examined samples served as the negative controlled sample. After culturing for 3, 6, and 24 h, the bacterial suspension was diluted 10 times and spread on the LB plate. The number of bacteria was determined by the colony counting method.

The bacterial inhibition rate was calculated based on the following equation: bacterial inhibition rate (%) = $(B - A)/B \times 100$; the antibacterial activity (R) was calculated by the equation: $R = \lg A - \lg B$, where A and B were pointed out to be the optical density of the negative controlled samples and tested samples, respectively. The release concentration for the Ag^+ from the Ag-$Sb_3P_2O_{14}$/PVDF films was quantitatively measured by inductively coupled plasma-optical emission spectroscopy (Agilent 720ES).

2.7. Stability and Durability Testing. Antibacterial membrane washing method of Shanghai University was used to test the washing durability of the Ag-$Sb_3P_2O_4$/PVDF film. The total liquid volume is 50 mL, including standard detergent

https://doi.org/10.1021/acsomega.2c02718
ACS Omega 2022, 7, 33858−33865

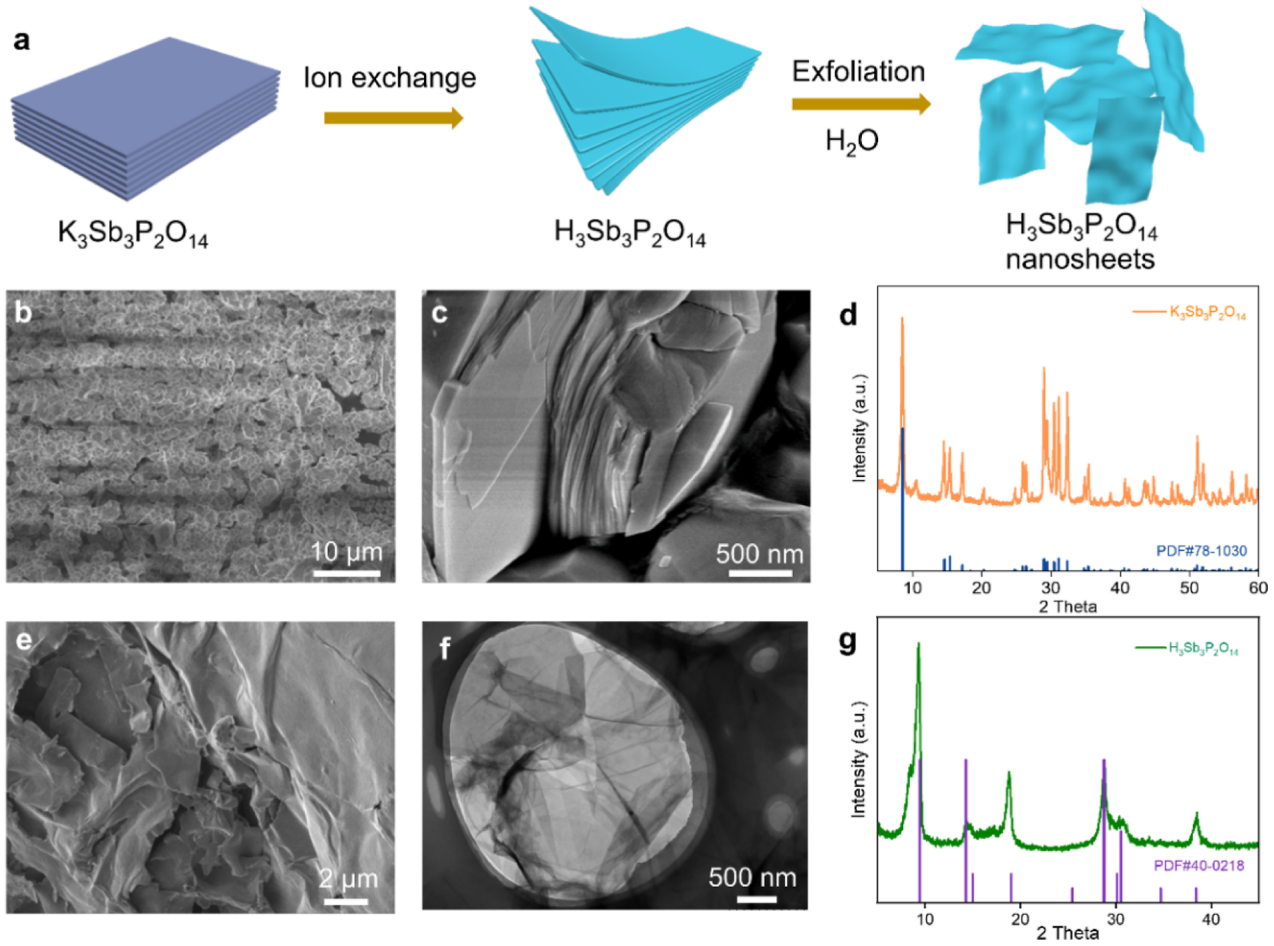

Figure 1. (a) Schematic of the synthesis strategy of $H_3Sb_3P_2O_{14}$. (b) Low magnification top-view SEM image and (c) enlarged image of $K_3Sb_3P_2O_{14}$. (d) XRD pattern of $K_3Sb_3P_2O_{14}$. (e) SEM and (f) TEM images of $H_3Sb_3P_2O_{14}$. (g) XRD pattern of $H_3Sb_3P_2O_{14}$.

ECE 2 g/L and 10 steel balls. Then, the Ag-$Sb_3P_2O_4$/PVDF thin film was put in it and kept at 40 °C for 45 min, washed twice with water at 40 °C (1 min each time), and finally dried.

3. RESULTS AND DISCUSSION

2D $Sb_3P_2O_{14}^{3-}$ nanosheets play an important role in adsorbing the Ag ions and controlling the slow release of Ag ions, which was synthesized through a "top-down" strategy,[27] as shown in Figure 1a. First, bulk $K_3Sb_3P_2O_{14}$ with a layer crystal structure was prepared by a conventional solid-phase method. SEM image shows the particle-like morphology with microsize (Figure 1b), and the enlarged SEM image reveals the layer-stacked structure of the big particles, which is similar to that of bulk MXenes (Figure 1c). The XRD pattern confirms the $K_3Sb_3P_2O_{14}$ phase because the main diffraction peaks are indexed to $K_3Sb_3P_2O_{14}$ (JCPDS 78-1030), as shown in Figure 1d. Afterward, 3D $H_3Sb_3P_2O_{14}$ bulks can be obtained by immersing the bulk $K_3Sb_3P_2O_{14}$ into nitric acid, followed by centrifugation and exfoliation. The XRD result also confirmed the successful transition from $K_3Sb_3P_2O_{14}$ to $H_3Sb_3P_2O_{14}$, indicating the successful ion-exchange reaction (Figure 1g). The obtained $H_3Sb_3P_2O_{14}$ bulk was further exfoliated, and the desired 2D $H_3Sb_3P_2O_{14}$ nanosheets were obtained through simple mechanical agitation in aqueous solution, which was confirmed by the SEM and TEM images. As displayed in Figure 1e, the SEM image shows the micro-sized sheetlike nanostructures. TEM further reveals its 2D graphene-like nanosheet morphology (Figure 1f).

The 2D $H_3Sb_3P_2O_{14}$ nanosheets are easily and uniformly dispersed in H_2O to form a homogeneous and transparent suspension (Figure 2a). In aqueous solution, 2D $H_3Sb_3P_2O_{14}$ nanosheets are easy to form 2D $Sb_3P_2O_{14}^{3-}$ anionic nanosheets with a rich negatively charge via ionization.[27] Because of strong electrostatic repulsions between nanosheets, the colloidal suspension of 2D $H_3Sb_3P_2O_{14}$ nanosheets is very stable. In order to obtain Ag-$Sb_3P_2O_{14}$ nanosheets, $AgNO_3$ was added to the colloidal suspension, where the positively charged Ag^+ are attracted by the negatively charged nanosheets by electrostatic interactions (Figure 2a,b). The SEM with the corresponding EDS mapping images of the nanosheets verify that the Ag ions have been adsorbed on the 2D $Sb_3P_2O_{14}^{3-}$ nanosheets. As shown in Figure 2c, the surface of nanosheets becomes rough. The EDS mapping shows the uniform distribution of Ag, N, O, P, and Sb elements. The presence of N element is attributed to NO^{3-} adsorption. The EDS spectrum shows that the mass loading of Ag is as high as 33.4 wt %, indicating high adsorption of Ag ions (Figure 2c). Furthermore, the XRD pattern of Ag-$Sb_3P_2O_{14}$ shows that all main diffraction peaks are indexed to the phase of $H_3Sb_3P_2O_{14}$ (JCPDS 40-0218), indicating that the adsorbed Ag ion compound is amorphous (Figure 2d). Besides, XPS spectra shows a strong Ag 3d peak, indicating the presence of Ag in the Ag-$Sb_3P_2O_{14}$ nanosheets. The corresponding high-resolution peaks were well fitted to

https://doi.org/10.1021/acsomega.2c02718
ACS Omega 2022, 7, 33858−33865

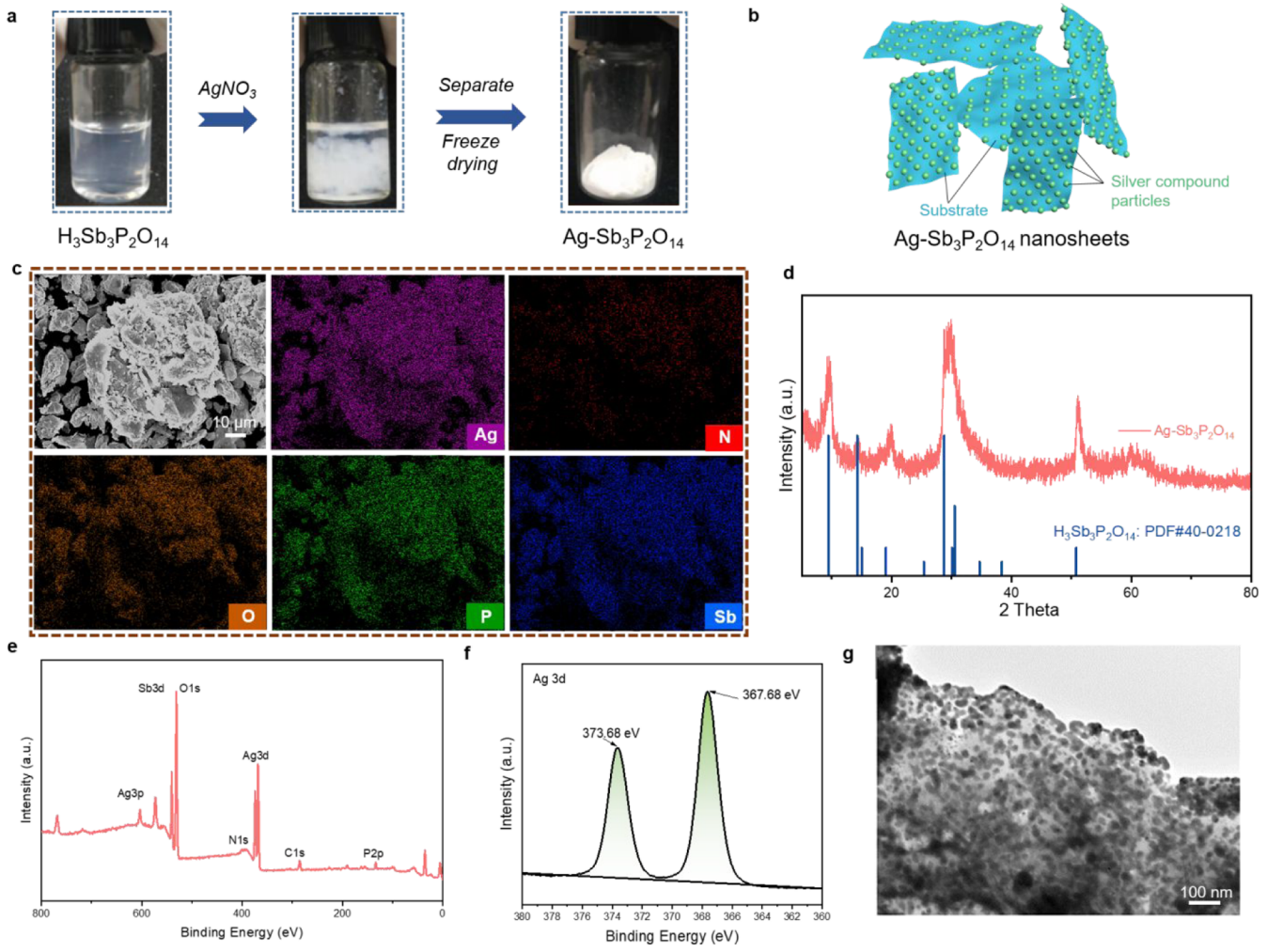

Figure 2. (a) Preparation of Ag-$Sb_3P_2O_{14}$ powder. (b) Schematic diagram of Ag-$Sb_3P_2O_{14}$ nanosheets. (c) Top-view SEM image and EDS map obtained from the Ag-$Sb_3P_2O_{14}$ powder. (d) XRD pattern of Ag-$Sb_3P_2O_{14}$ powder. (e,f) XPS spectra of Ag-$Sb_3P_2O_{14}$ powder: (e) survey scan and (f) Ag 3d. (g) TEM image of Ag-$Sb_3P_2O_{14}$ powder.

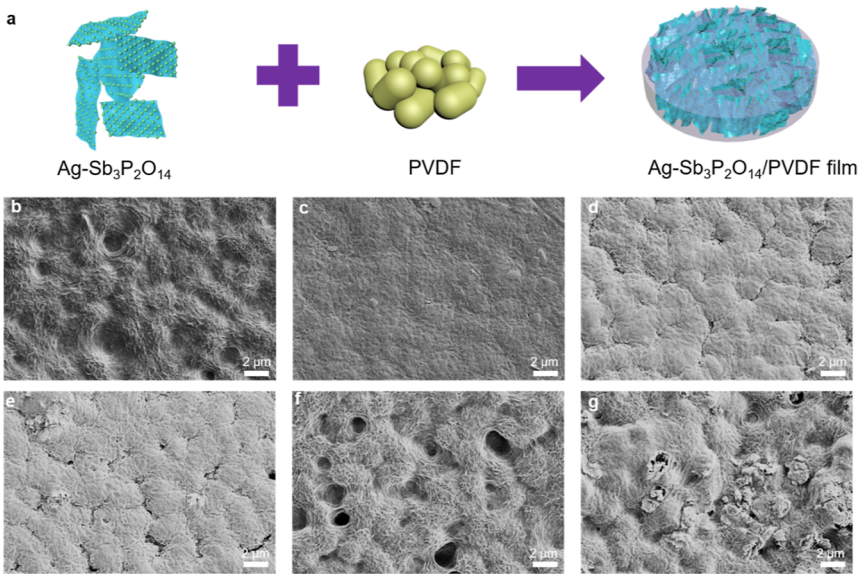

Figure 3. (a) Schematic of the synthesis strategy of Ag-$Sb_3P_2O_{14}$/PVDF film. Top-view SEM images of the (b) PVDF film with 10 wt % $H_3Sb_3P_2O_{14}$ film, (c) pure PVDF film, and PVD film with (d) 5 wt % Ag-$Sb_3P_2O_{14}$, (e) 10 wt % Ag-$Sb_3P_2O_{14}$, (f) 15 wt % Ag-$Sb_3P_2O_{14}$, and (g) 20 wt % Ag-$Sb_3P_2O_{14}$.

https://doi.org/10.1021/acsomega.2c02718
ACS Omega 2022, 7, 33858−33865

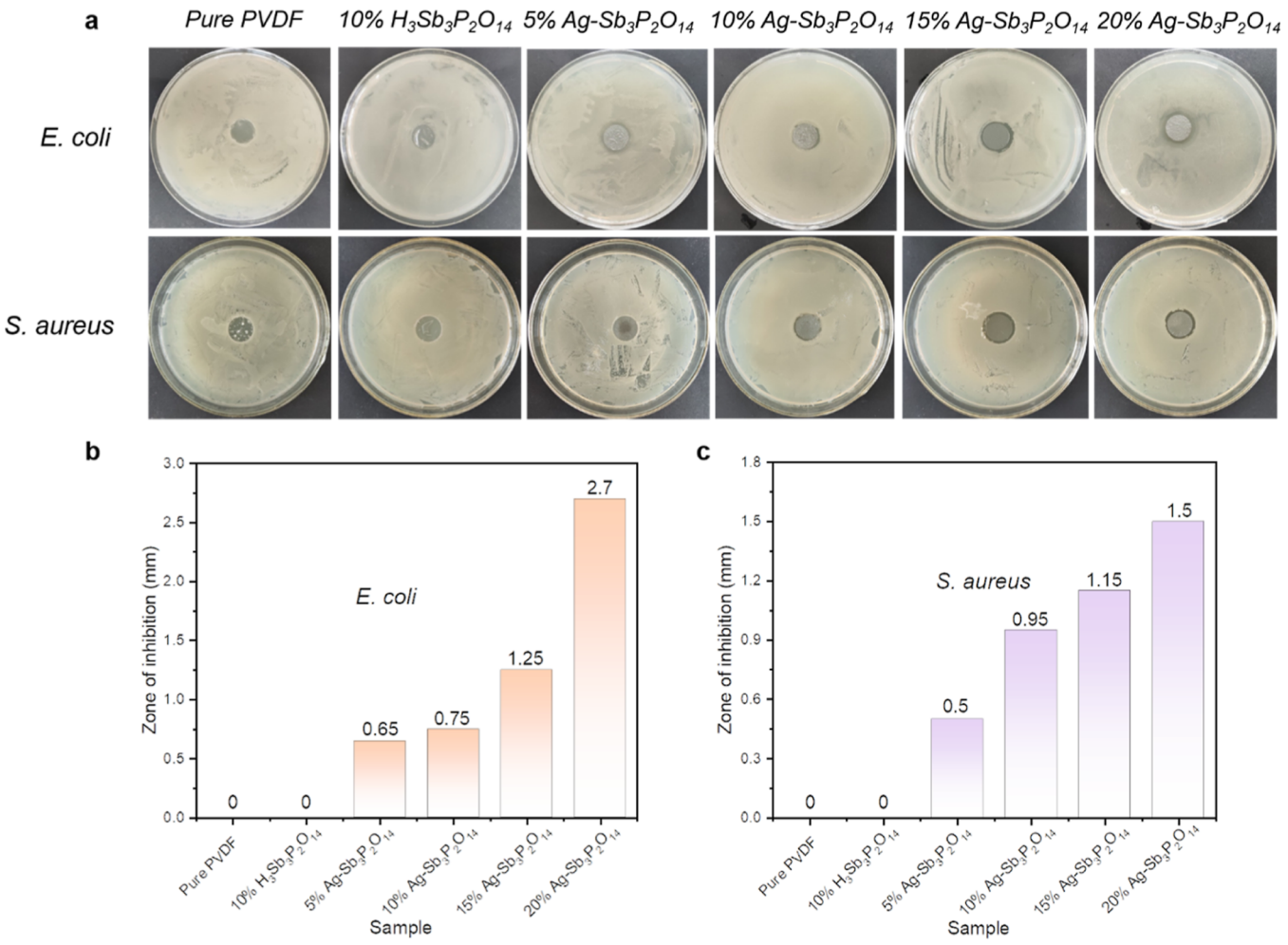

Figure 4. (a–c) Inhibition zone of (b) *E. coli* and (c) *S. aureus* of pure PVDF, 10 wt % $H_3Sb_3P_2O_{14}$, 5 wt % Ag-$Sb_3P_2O_{14}$/PVDF, 10 wt % Ag-$Sb_3P_2O_{14}$/PVDF, 15 wt % Ag-$Sb_3P_2O_{14}$/PVDF, and 20 wt % Ag-$Sb_3P_2O_{14}$/PVDF.

the Ag $d_{3/2}$ orbital (373.68 eV) and the Ag $d_{5/2}$ orbital (367.68 eV), further confirming that Ag (I) existed in the Ag-$Sb_3P_2O_{14}$ nanosheets rather than metal Ag (0) (Figure 2e,f).[29] Compared with $AgNO_3$ chelated by poly(2-ethyl-2-oxazoline), the lower binding energy of valence electrons of Ag in Ag-$Sb_3P_2O_{14}$ nanosheets demonstrated the weaker interaction between the silver cation and the substrate, which is beneficial to the release of Ag ions.[29] Moreover, the TEM image reveals that the nanoparticle-like Ag^+ compound including NO_3^- ($AgNO_3$) is uniformly dispersed on the nanosheets in the form of nanoparticles, which is consistent with the EDS results (Figure 2g).

To improve the antibacterial activity of the PVDF film, Ag-$Sb_3P_2O_{14}$ served as the nanofiller to prepare the PVDF composite film by the way of solution blending, as shown in Figure 3a. SEM was used to investigate the morphology of the PVDF film with different loadings of Ag-$Sb_3P_2O_{14}$ nanofillers (Figure 3b–g). Obviously, pure PVDF membrane displays a flat and dense surface without obvious pores or undulation (Figure 3c). After incorporating 5 wt % Ag-$Sb_3P_2O_{14}$, the surface became a little rough, and no big aggregate of Ag-$Sb_3P_2O_{14}$ was found, indicating its good dispersion (Figure 3d). It was found that the surface roughness of the composite membrane increased with the increase of Ag-$Sb_3P_2O_{14}$. With a very high loading of Ag-$Sb_3P_2O_{14}$ as high as 20 wt %, some Ag-$Sb_3P_2O_{14}$ aggregates were detected because of the high loading of fillers. For comparison, the PVDF membrane with 10 wt % $H_3Sb_3P_2O_{14}$ nanosheets was prepared, showing a rough surface (Figure 3b). It should be noted that no $H_3Sb_3P_2O_{14}$ aggregates were detected with the loading of 10 wt % $H_3Sb_3P_2O_{14}$ nanosheets.

In order to evaluate the antibacterial activities of the Ag-$Sb_3P_2O_{14}$/PVDF film, the zone of inhibition tests were conducted first, where the diameter of the round films was 0.02 m. As displayed in Figure 4a, pure PVDF films did not show any inhibition zone for both *E. coli* and *S. aureus*, indicating that the pure PVDF film cannot kill the bacterial around the film. In contrast, it could be observed that the PVDF composite samples with Ag-$Sb_3P_2O_{14}$ nanosheets demonstrated antibacterial effect for both *E. coli* and *S. aureus*, confirming the important role of the Ag-$Sb_3P_2O_{14}$ nanosheets on the antibacterial performance. In detail, with the increasing of the content of Ag-$Sb_3P_2O_{14}$ in the films, the diameter of the corresponding inhibition zones increases (Figure 4b,c). The diameter is as high as 2.7 mm for *E. coli* and 1.5 mm for *S. aureus* for the 20 wt % Ag-$Sb_3P_2O_{14}$/PVDF film, proving a strong connection between the Ag content and the antibacterial activity. It should be noted that the diameter of the inhibition zone is not high, indicating the slow release of Ag ions from the Ag-$Sb_3P_2O_{14}$ nanosheets.

Moreover, the standard plate count method was applied to quantitatively assess the antibacterial activity for the above Ag-

https://doi.org/10.1021/acsomega.2c02718
ACS Omega 2022, 7, 33858–33865

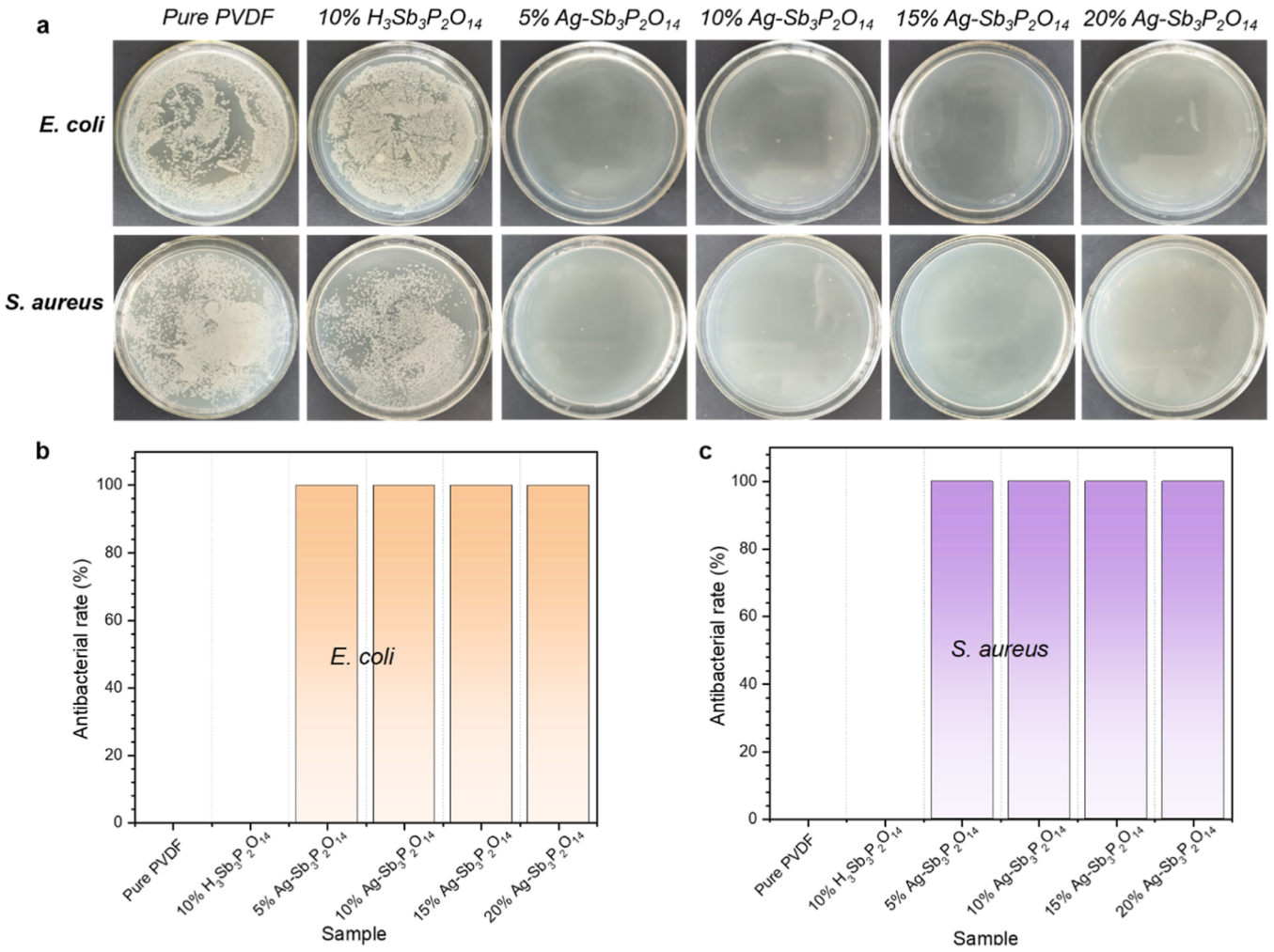

Figure 5. (a–c) Antibacterial rate of (b) *E. coli* and (c) *S. aureus* of PVDF films with 10 wt % $H_3Sb_3P_2O_{14}$, 5 wt % Ag-$Sb_3P_2O_{14}$/PVDF, 10 wt % Ag-$Sb_3P_2O_{14}$/PVDF, 15 wt % Ag-$Sb_3P_2O_{14}$/PVDF, and 20 wt % Ag-$Sb_3P_2O_{14}$/PVDF.

$Sb_3P_2O_{14}$/PVDF film. The results of the *E. coli* and *S. aureus* colonies with 7×10^6 CFU/mL concentration on the scaffolds have been displayed in Figure 5a. Obviously, the pure PVDF and 10 wt % $H_3Sb_3P_2O_{14}$/PVDF samples still maintained tons of bacteria on the surface of samples, expressing extremely low bacterial activities for both *E. coli* and *S. aureus*. However, after mixing the Ag-$Sb_3P_2O_{14}$ nanosheets into the composite film, the bacterial inhibition performance was hugely enhanced. All PVDF films with Ag-$Sb_3P_2O_{14}$ showed over 99.99% antibacterial rate (Figure 5b,c), which may be attributed to the excellent antibacterial activity of Ag-$Sb_3P_2O_{14}$ nanosheets.

The Ag^+ release evaluation of Ag-$Sb_3P_2O_{14}$ nanosheets was carried out by measuring the concentration of Ag ions as a function of rest time, as displayed in Figure 6a. Initially, 0.1 mg/mL Ag-$Sb_3P_2O_{14}$ nanosheets were suspended in the water solution and then placed for monitoring the concentration of Ag ions. After 3 days, the above solution has a Ag^+ concentration as high as 0.54 mg/L, indicating that the Ag-$Sb_3P_2O_{14}$ nanosheets can effectively release the Ag ions, which is higher than the concentration (from 0.1 to 10 μg/mL) the bacteria could live and could effectively inhibit the bacterial growth and reproduction.[30] This also explains that the films with a low loading of Ag-$Sb_3P_2O_{14}$ shows excellent antibacterial activities (Figure 6c). Remarkably, with the prolongation of rest time, the Ag^+ cumulative concentration gradually and slowly increases. The concentration of Ag ions is about 0.65 mg/L after placing for 5 days and is up to 0.90 mg/L after 7 days, verifying the excellent ability to slowly release Ag ions and ensuring the long-term antibacterial performance. Moreover, in order to detect the durable antibacterial performance of Ag-$Sb_3P_2O_{14}$ nanosheets, the antibacterial activity of the PVDF film with 5 wt % Ag-$Sb_3P_2O_{14}$ was examined after different washing times (Figure 6b). As shown in Figure 6b, the composite film exhibited a high antibacterial performance and kills almost all *E. coli* and *S. aureus* even after washing 50 times, confirming its durable antibacterial activity of the PVDF based films. The excellent durable antibacterial effect of Ag-$Sb_3P_2O_{14}$/PVDF film against *E. coli* and *S. aureus* is attributed the ability of the slow release of Ag ions for the Ag-$Sb_3P_2O_{14}$ nanosheets.

4. CONCLUSIONS

In summary, we have designed and prepared a new Ag-based antibacterial agent, which is composed of 2D Ag-$Sb_3P_2O_{14}$ nanosheets. 2D anionic nanosheets can load large amounts of Ag ions on the surface through electrostatic interactions, which also control the slow release of surface Ag ions in aqueous solution. Inductively coupled plasma–optical emission spectrometry results reveal that the concentration of Ag ions of the solution containing 2D Ag-$Sb_3P_2O_{14}$ nanosheets increase with

https://doi.org/10.1021/acsomega.2c02718
ACS Omega 2022, 7, 33858–33865

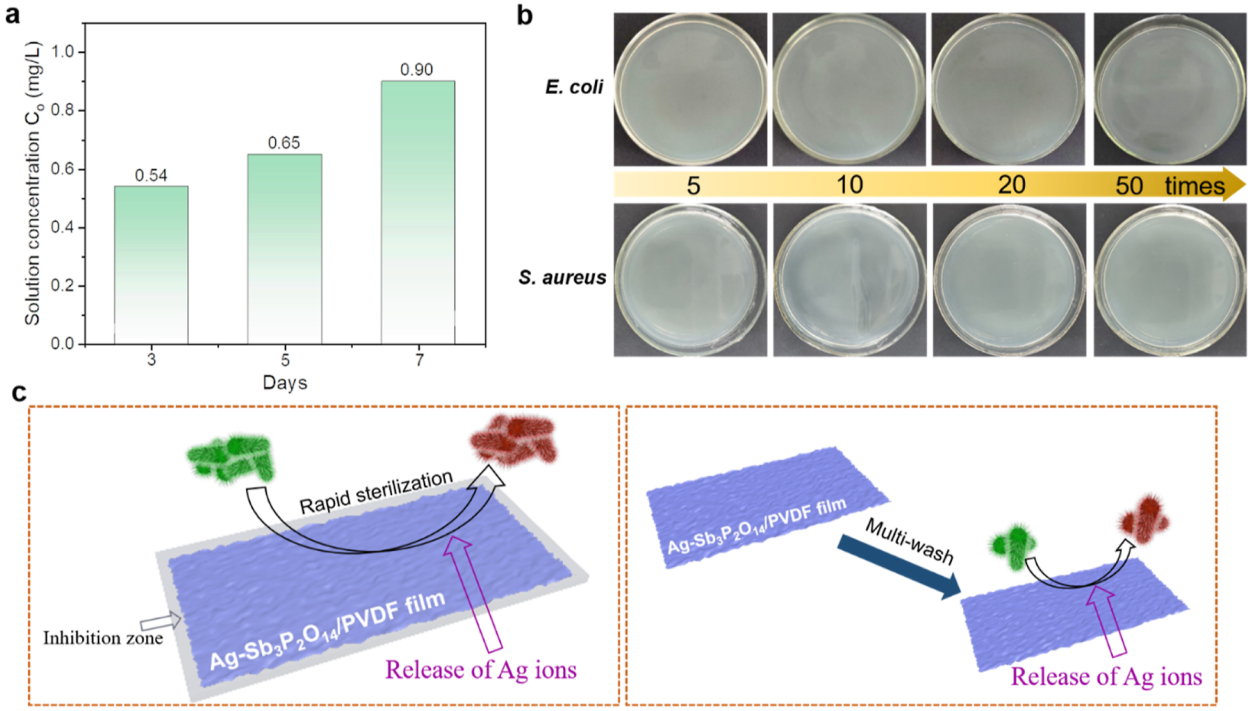

Figure 6. (a) Release concentration of Ag ions of PVDF with 5 wt % Ag-$Sb_3P_2O_{14}$. (b) Antimicrobial activities against *E. coli* and *S. aureus* of the PVDF film with 5 wt % Ag-$Sb_3P_2O_{14}$ after different washing times. (c) Proposed mechanism schematic of Ag-$Sb_3P_2O_{14}$/PVDF films.

an increase of the soaking time, exhibiting outstanding continuous sterilization performance. The as-prepared 2D Ag-$Sb_3P_2O_{14}$ nanofillers enable the PVDF membrane with high antibacterial activities against both *E. coli* and *S. aureus* (over 99.99% antibacterial rate). Besides, it should be noted that the antibacterial ability of the PVDF film with 5 wt % 2D Ag-$Sb_3P_2O_{14}$ nanosheets remains high antibacterial effect after 50 times washing, further confirming the slow release of Ag ions anchored on the 2D anionic nanosheets. Such distinguished antibacterial activities of the Ag-$Sb_3P_2O_{14}$/PVDF film indicate the application potential to develop polymer-based composites with durable antimicrobial activities against microorganisms.

AUTHOR INFORMATION

Corresponding Authors

Chao Wu − *School of Environmental and Chemical Engineering, Shanghai University, Shanghai 200444, China; Institute for Superconducting & Electronic Materials, Australian Institute of Innovative Materials, University of Wollongong, New South Wales 2522, Australia;* orcid.org/0000-0002-2825-6337; Email: klyan@dhu.edu.cn

Ke-lu Yan − *College of Chemistry, Chemical Engineering and Biotechnology, Donghua University, Shanghai 201620, China*; Email: chaowu@uow.edu.au

Authors

Shi-Yu Yang − *College of Chemistry, Chemical Engineering and Biotechnology, Donghua University, Shanghai 201620, China*

Kuan Wu − *School of Environmental and Chemical Engineering, Shanghai University, Shanghai 200444, China*

Ying Zhang − *School of Environmental and Chemical Engineering, Shanghai University, Shanghai 200444, China*

Hao-Xuan Liu − *Institute for Superconducting & Electronic Materials, Australian Institute of Innovative Materials, University of Wollongong, New South Wales 2522, Australia;* orcid.org/0000-0003-2402-9679

Ping Li − *School of Life Sciences, Shanghai University, Shanghai 200444, PR China*

Complete contact information is available at: https://pubs.acs.org/10.1021/acsomega.2c02718

Notes

The authors declare no competing financial interest.

ACKNOWLEDGMENTS

The authors greatly acknowledge the support from the Science and Technology Commission of Shanghai Municipality (20010500400). The authors also thank for the help from Xiu Shen in the antibacterial test.

REFERENCES

(1) Liu, F.; Hashim, N. A.; Liu, Y. T.; Abed, M. R. M.; Li, K. Progress in the production and modification of PVDF membranes. *J. Membr. Sci.* **2011**, *375*, 1−27.

(2) Kang, G. D.; Cao, Y. M. Application and modification of poly(vinylidene fluoride) (PVDF) membranes - A review. *J. Membr. Sci.* **2014**, *463*, 145−165.

(3) Wang, A.; Shao, M. W.; Yang, F.; Shao, C. K.; Chen, C. F. Preparation and properties of antibacterial PVDF composite thin films. *Eur. Polym. J.* **2021**, *160*, 110803.

(4) Ray, S. S.; Dangayach, R.; Kwon, Y. N. Surface engineering for anti-wetting and antibacterial membrane for enhanced and fouling resistant membrane distillation performance. *Chem. Eng. J.* **2021**, *405*, 126702.

(5) Pan, Y.; Yu, Z. X.; Shi, H.; Chen, Q.; Zeng, G. Y.; Di, H. H.; Ren, X. Q.; He, Y. A novel antifouling and antibacterial surface-functionalized PVDF ultrafiltration membrane via binding Ag/SiO2 nanocomposites. *J. Chem. Technol. Biotechnol.* **2017**, *92*, 562.

(6) Baji, A.; Truong, V. K.; Gangadoo, S.; Yin, H.; Chapman, J.; Abtahi, M.; Oopath, S. V. Durable Antibacterial and Antifungal Hierarchical Silver-Embedded Poly(vinylidene fluoride-co-hexafluoropropylene) Fabricated Using Electrospinning. *ACS Appl. Polym. Mater.* **2021**, *3*, 4256−4263.
(7) Geng, C. B.; Fan, L. A.; Niu, H. Y.; Liu, L. J.; Zhao, F. B.; Zhang, J. M.; Dong, H. X.; Yu, S. L. Improved anti-organic fouling and antibacterial properties of PVDF ultrafiltration membrane by one-step grafting imidazole-functionalized graphene oxide. *Mater. Sci. Eng., C* **2021**, *131*, 112517.
(8) Ayyaru, S.; Pandiyan, R.; Ahn, Y. H. Antibacterial and Adsorption Properties of Sulfonated GO-PVDF Nanocomposite Ultrafiltration Membranes for Environmental Applications. *J. Environ. Eng.* **2021**, *147* (10), 04021042.
(9) Liu, H. S.; Liu, X. Y.; Zhao, F. B.; Liu, Y.; Liu, L. J.; Wang, L. H.; Geng, C. B.; Huang, P. Preparation of a hydrophilic and antibacterial dual function ultrafiltration membrane with quaternized graphene oxide as a modifier. *J. Colloid Interface Sci.* **2020**, *562*, 182−192.
(10) Centa, U. G.; Sternisa, M.; Visic, B.; Federl, Z.; Mozina, S. S.; Remskar, M. Novel nanostructured and antimicrobial PVDF-HFP/PVP/MoO3 composite. *Surf. Innovations* **2021**, *9*, 256−266.
(11) Jin, G. W.; Kim, J. Y.; Min, B. G. Superhydrophobic and Antibacterial Properties of Cotton Fabrics Treated with PVDF and nano-ZnO through Phase Inversion Process. *Fibers Polym.* **2018**, *19*, 1835−1842.
(12) Damodar, R. A.; You, S. J.; Chou, H. H. Study the self cleaning, antibacterial and photocatalytic properties of TiO2 entrapped PVDF membranes. *J. Hazard. Mater.* **2009**, *172*, 1321−8.
(13) Muñoz-Bonilla, A.; Kubacka, A.; Fernández-García, M.; Ferrer, M.; Fernández-García, M.; Cerrada, M. L. Visible and ultraviolet antibacterial behavior in PVDF-TiO2 nanocomposite films. *Eur. Polym. J.* **2015**, *71*, 412−422.
(14) Cho, K. Y.; Yoo, C. H.; Won, Y. J.; Hong, D. Y.; Chang, J. S.; Choi, J. W.; Lee, J. H.; Lee, J. S. Surface-concentrated chitosan-doped MIL-100(Fe) nanofiller-containing PVDF composites for enhanced antibacterial activity. *Eur. Polym. J.* **2019**, *120*, 109221.
(15) Zheng, H.; Wang, D.; Sun, X.; Jiang, S.; Liu, Y.; Zhang, D. Q.; Zhang, L. Z. Surface modified by green synthetic of Cu-MOF-74 to improve the anti-biofouling properties of PVDF membranes. *Chem. Eng. J.* **2021**, *411*, 128524.
(16) Al-Sherbini, A.-S. A.; Ghannam, H. E. A.; El-Ghanam, G. M. A.; El-Ella, A. A.; Youssef, A. M. Utilization of chitosan/Ag bionanocomposites as eco-friendly photocatalytic reactor for Bactericidal effect and heavy metals removal. *Heliyon* **2019**, *5*, No. e01980.
(17) Qing, Y. A.; Cheng, L.; Li, R. Y.; Liu, G. C.; Zhang, Y. B.; Tang, X. F.; Wang, J. C.; Liu, H.; Qin, Y. G. Potential antibacterial mechanism of silver nanoparticles and the optimization of orthopedic implants by advanced modification technologies. *Int. J. Nanomed.* **2018**, *13*, 3311−3327.
(18) Le Ouay, B.; Stellacci, F. Antibacterial activity of silver nanoparticles: A surface science insight. *Nano Today* **2015**, *10*, 339−354.
(19) Jiang, H. S.; Zhang, Y. Z.; Lu, Z. W.; Lebrun, R.; Gontero, B.; Li, W. Interaction between Silver Nanoparticles and Two Dehydrogenases: Role of Thiol Groups. *Small* **2019**, *15*, No. e1900860.
(20) Shuai, C. J.; Guo, W.; Wu, P.; Yang, W. J.; Hu, S.; Xia, Y.; Feng, P. A graphene oxide-Ag co-dispersing nanosystem: Dual synergistic effects on antibacterial activities and mechanical properties of polymer scaffolds. *Chem. Eng. J.* **2018**, *347*, 322−333.
(21) Lu, Z.; Gao, J. T.; He, Q. F.; Wu, J.; Liang, D. H.; Yang, H.; Chen, R. Enhanced antibacterial and wound healing activities of microporous chitosan-Ag/ZnO composite dressing. *Carbohydr. Polym.* **2017**, *156*, 460−469.
(22) Qin, C.; Zhang, M.; Li, B.; Li, Y.; Wang, Z. Ag particles modified CuxO (x=1, 2) nanowires on nanoporous Cu-Ag bimetal network for antibacterial applications. *Mater. Lett.* **2020**, *258*, 126823.
(23) Saedi, S.; Shokri, M.; Priyadarshi, R.; Rhim, J. W. Silver ion loaded 3-aminopropyl trimethoxysilane -modified Fe3O4 nanoparticles for the fabrication of carrageenan-based active packaging films. *Colloids Surf., B* **2021**, *208*, 112085.
(24) Chang, L.; Duan, W. J.; Chen, A. G.; Li, J. J.; Huang, S. Q.; Tang, H. J.; Pan, G.; Deng, Y.; Zhao, L. N.; Li, D. F.; Zhao, L. Preparation of polyacrylonitrile-based fibres with chelated Ag ions for antibacterial applications. *R. Soc. Open Sci.* **2020**, *7*, 200324.
(25) Rivas, B. L.; Pereira, E.; Guzman, C.; Maureira, A. In Complexes of Water-Soluble Polymers with Cu2+ and Ag+ as Antibacterial Agents. *13th IUPAC International Symposium on Macromoleculer Complexes (MMC), Termas de Chillan, CHILE, Nov 15-17; Termas de Chillan, CHILE*, 2009; pp 46−54.
(26) Saedi, S.; Shokri, M.; Priyadarshi, R.; Rhim, J.-W. Silver ion loaded 3-aminopropyl trimethoxysilane -modified Fe3O4 nanoparticles for the fabrication of carrageenan-based active packaging films. *Colloids Surf., B* **2021**, *208*, 112085.
(27) Zhang, Y.; Zhu, M.; Wang, G. Y.; Du, F. H.; Yu, F. F.; Wu, K.; Wu, M. H.; Dou, S. X.; Liu, H. K.; Wu, C. Dendrites-Free Zn Metal Anodes Enabled by an Artificial Protective Layer Filled with 2D Anionic Nanosheets. *Small Methods* **2021**, *5*, 2100650.
(28) Szendrei, K.; Ganter, P.; Sànchez-Sobrado, O.; Eger, R.; Kuhn, A.; Lotsch, B. V. Touchless Optical Finger Motion Tracking Based on 2D Nanosheets with Giant Moisture Responsiveness. *Adv. Mater.* **2015**, *27*, 6341−6348.
(29) Kang, S. W.; Kim, J. H.; Char, K.; Kang, Y. S. Chemical Activation of AgNO3 to Form Olefin Complexes Induced by Strong Coordinative Interactions with Phthalate Oxygens of Poly(ethylene phthalate). *Ind. Eng. Chem. Res.* **2006**, *45*, 4011−4014.
(30) Sukhorukova, I. V.; Sheveyko, A. N.; Shvindina, N. V.; Denisenko, E. A.; Ignatov, S. G.; Shtansky, D. V. Approaches for Controlled Ag+ Ion Release: Influence of Surface Topography, Roughness, and Bactericide Content. *ACS Appl. Mater. Interfaces* **2017**, *9*, 4259−4271.

https://doi.org/10.1021/acsomega.2c02718
ACS Omega 2022, 7, 33858−33865